Running title

Meristems in lateral organs

Title

Differed cell division angle, position of cell proliferative area, and localization of ANGUSTIFOLIA3 in lateral organs

Authors

Ayaka Kinoshita[1*], Makiko Naito[1*], Hirokazu Tsukaya[1]

*Contributed equally to this work

Affiliations

[1]Graduate School of Science, The University of Tokyo, Tokyo, Japan

Correspondence

Corresponding Author: Hirokazu Tsukaya

Contact: tsukaya@bs.s.u-tokyo.ac.jp

Word counts & number of figures

Total (main body): 5,730 words

Introduction: 993 words

Materials and Methods: 1,156 words

Results: 1,514 words

Discussion: 2,067 words

Number of figures: 11

Number of supporting information: 1Summary statement

Different lateral organs with different morphology possess different properties of meristems; cell division angles, position of cell proliferative area and AN3 localization patterns.

Abstract

Leaf meristem is a cell proliferative zone present in the lateral organ primordia. In this study, we investigated how the proliferative zone affects the final morphology of the lateral organs. We examined how cell proliferative zones differ in the primordia of planar floral organs and polar auxin transport inhibitor (PATI)-treated leaves from normal foliage leaf primordia of

Arabidopsis thaliana with a focus on the spatial accumulation pattern of *ANGUSTIFOLIA3* (*AN3*), a key element for leaf meristem positioning. We found that organ shape changes by PATI treatment were correlated to the angle of the cell division plane relative to the leaf primordia axis in the leaf meristem (cell division angle), but not with leaf-meristem positioning, size of the leaf meristem, or the localization pattern of AN3 protein. In contrast, different shapes between sepals and petals compared with foliage leaves were associated with both altered meristem position associated with altered *AN3* expression patterns and different distributions of cell division angles. These results suggest that lateral organ shapes are regulated via two aspects: position of meristem and cell division angles

Key words

AN3, cell division, lateral organ, leaf meristem, morphology, polar auxin transport inhibitor

Introduction

The shape of leaves plays an important role in determining their photosynthetic function. Moreover, the shape of floral organs, which are evolutionarily derived from leaves, is also important for reproductive success. Therefore, the shape of these lateral organs varies among species to maximize their survival ability in their natural habitats. To understand these variations, it is important to assess their developmental properties.

The center of morphogenesis in plants is the meristem, where active cell division occurs. The shoot apical meristem (SAM) is essential to produce new above-ground organs. In terms of lateral organs, especially for leaf primordia, the leaf meristem supplies cells to the leaf blade; thus, researchers have investigated the nature of the meristem to understand the morphogenesis of lateral organs (e.g. Esau, 1977; Donnelly et al., 1999; Kazama et al., 2010; Ichihashi et al., 2011).

In many angiosperms, such as *Arabidopsis thaliana*, the leaf meristem is at the base of each leaf (Tsukaya, 2014; 2021). Cell proliferation initially occurs throughout the leaf primordium but is restricted to its basal regions as the leaf primordium grows further (Donnelly et al., 1999; Kazama et al., 2010). The control on the restriction of the cell proliferation zone is not completely understood. However, a transcriptional coactivator called ANGUSTIFOLIA3 (AN3)/GRF-INTERACTING FACTOR1 (GIF1), which encodes a protein that is homologous to the human synovial sarcoma translocation protein (Horiguchi et al., 2005), is considered to positively control cell proliferation in leaf primordia. The spatial patterns of AN3/GIF1 (simplified to AN3, hereafter) accumulation at the base of leaf primordia match the cell

proliferation zone, suggesting that AN3 may act as an important determinant in positioning the leaf meristem (Horiguchi et al., 2005; Kawade et al., 2017). Cell division angles in the *AN3*-expressing region, except for areas along the margin and vasculature, were observed to be randomized (Yin and Tsukaya, 2016), which may contribute to the two-dimensional expansion of the leaf lamina. AN3 protein moves cell-to-cell (Kawade et al., 2013), forms a gradient along the proximal-distal axis on the leaf, with the leaf base presenting the highest concentration of AN3 protein (Kawade et al., 2017) and thus is involved in the positioning of the leaf meristem. However, how *AN3* expression is restricted to the basal part of leaf primordia is still unknown (Tsukaya, 2021).

AN3 seems to be also involved in the morphogenesis of each floral organ (Lee et al., 2009, 2014). A petal in the *an3* mutant has a smaller number of cells and a narrower shape than that of the wild type (Lee et al., 2009), as seen in the foliage leaves, suggesting a common role of AN3 in leaf and petal primordia. However, the past studies indicated that the position of the meristematic activity in the petal primordia is marginal/apical in *A. thaliana* (*e.g.,* Dinneny et al., 2004), which is clearly different from the leaf primordia. Precisely said, the cell proliferation is observed in the entire primordia of the petal organ at first, and then in the distal region in later stages, differed from that of leaf primordia (Disch et al., 2006; Anastasiou et al., 2007). Thus, if AN3 has the same role in the positional determination of the meristematic zone in petal primordia, AN3 proteins are expected to accumulate apically and not basally in petal primordia; however, no previous studies have examined it. Marginal/apical positioning of the meristematic zone in petals may be an ancestral character that is directly comparable to the apical positioning of SAM (Boyce, 2007). Although the basal positioning of the leaf meristem is common in angiosperms, marginal/apical positioning in leaf primordia is also known in some ferns and gymnosperms. Therefore, a comparison of leaf primordia with floral organ primordia of the same species, with special emphasis on *AN3* expression, may contribute toward understanding the roles and evolutionary history of differences in the positioning of cell proliferation activity in the primordia of these lateral organs.

In relation to the above-mentioned positioning of the meristematic zones in lateral organs, venation pattern is also an evident difference between the leaves of angiosperms, ferns, and gymnosperms (Boyce, 2007). In the lateral organs of ferns and gymnosperms harboring meristems along the apical margin, the leaf vein shows a bifurcated pattern and is open at the end. In contrast, lobed and closed patterns are common in eudicots including *A. thaliana*; parallel patterns are common in monocots (Dengler and Kang, 2001). Based on this correlation,

an interaction between spatial control of the leaf cell proliferation zone and leaf venation pattern has been suggested (Boyce, 2007).

How the spatial control of the leaf cell proliferation zone and leaf venation patterns are interconnected? In addition, are these indeed correlated? If we refer to the earlier-mentioned AN3, the cell division orientation is randomized in leaf meristem, where AN3 localized, except for the local regions along veins and leaf margin where active auxin flow is recognized (Yin and Tsukaya, 2016). This might suggest a missing link between the spatial control of the leaf cell proliferation zone and leaf venation pattern, but no prior studies have investigated this possibility.

In vein development in the leaf, biosynthesis and transportation of the plant hormone auxin (indole-3-acetic acid, IAA) plays an important role (Cheng et al., 2006). For example, *GNOM* and *PIN-FORMED* (*PIN*) genes that control polar auxin transport (PAT) (Verna et al., 2019) regulate vein formation during leaf development. Members of the PIN family have been extensively studied as major factors in PAT, the most famous being PIN1 (Okada et al., 1991). Mutations in many *PIN* genes induce defects in leaf vein patterns, with wide and bifurcated midveins and altered leaf blade shapes (Sawchuk et al., 2013). Similarly, mutants with an abnormal venation pattern mostly show altered leaf shapes in *A. thaliana* (Candela et al., 1999).

Many PAT inhibitors (PATIs) have been used to examine the role of PAT in plant organogenesis, including 2,3,5-triiodobenzoic acid (TIBA) and N-1-naphthylphthalamic acid (NPA). Through indirect evidence, they bind to the same auxin efflux carriers to inhibit their activity (Teale and Palme, 2018). When plants are treated with PATI, their leaves exhibit abnormal leaf venation patterns, including very thick midveins and marginal veins, similar to that of *pin1* mutants (Sieburth, 1999). In addition, the leaf shape becomes rounder and shorter than that of control plants. However, to date, no study has examined the effect of PATI on the cell proliferation pattern in leaf primordia.

To fully understand the morphogenesis process of lateral organs, it is necessary to investigate the role of the lateral organ meristem on the final organ shape and factors that affect the properties of meristems. In this study, we chose PATI-treated leaves and floral organs as models of leaves with altered morphology and venation pattern; and investigated the spatial position of cell proliferative area, cell division angle, and possible factors that control the properties of lateral organ meristems using AN3 as a key clue.

134 **Results**

135 Change in the length of cell proliferation zone

136 Firstly, we examined whether PATI treatment affects leaf shape via changes in leaf meristem
137 positioning in *A. thaliana.* In the PATI-treated plants, the leaves became shorter and rounder
138 than those of the control plants (**Figs. 1D-F**, **2**). The leaf vein pattern also differed in PATI-
139 treated leaves (**Fig. 1D-F**); namely, the midvein was widened, the lateral veins ran parallel to
140 each other, and the veins adjacent to leaf margins were also widened, indicating drastic changes
141 in leaf organogenesis. These observations are consistent with those of previous reports
142 (Mattsson et al., 1999; Sieburth, 1999; Sawchuk et al., 2013).

143 To investigate the effect of inhibition of PAT on the leaf meristem, the cell proliferation
144 zone was observed in the leaf primordia of PATI-treated plants. The *CYCB1;1::β-*
145 *glucuronidase* (*GUS*) line is used to visualize dividing G2-M phase cells (Donnelly et al., 1999).
146 The first and second rosette leaves of 6 days after sowing stage (DAS) seedlings for control
147 plants and 7 DAS seedlings for PATI-treated plants were used for this experiment, considering
148 the growth retardation observed in the PATI-treated plants.

149 In the PATI-treated plants, the cell proliferation zone remained in the proximal
150 position, similar to the control plants (**Fig. 1A-C**). The images were processed to further
151 examine the positioning of the cell proliferation zone (**Fig. 3**). We observed that both the length
152 of the cell proliferation zone from the leaf base and the ratio of cell proliferation zone to the
153 total leaf length were found to be increased in PATI-treated leaves (**Fig. 3C, D**).

154

155 *AN3* mRNA and AN3 protein localization in leaf primordia

156 To investigate how the length of the cell proliferation zone increased, we examined
157 the localization of *AN3* expression. As AN3 protein can move between cells, two lines, *an3-*
158 *4/pAtAN3::AN3-GREEN FLUORESCNT PROTEIN* (*GFP*) and *an3-4/pAtAN3::AN3-3xGFP*,
159 were used for the observation. The former can detect actual protein localization, whereas the
160 latter is used to monitor mRNA localization because it represents an accumulation of the
161 protein without cell-to-cell movement ability (Kawade et al., 2013, 2017). The first and second
162 rosette leaves of 5 DAS seedlings were used for this analysis.

163 We observed that the overall localization of AN3 under PATI treatment did not change
164 from that of the control; it remained in the proximal region (**Fig. 4A-L**). This confirms the
165 observation in the cell proliferation zone described above. The size of the *AN3*-expressing
166 regions was also measured using the same image processing method used for the analysis of
167 the cell proliferation zone. Consequently, the *AN3*-mRNA expressing regions, monitored by

168 the presence of the AN3-3xGFP signal, were slightly longer in the PATI-treated leaves than in
169 control (**Fig. 4M**). However, AN3 protein localization of TIBA- or NPA-treated plants did not
170 show a statistical difference from that of control plants (**Fig. 4M**). Therefore, irrespective of
171 changes in *AN3* mRNA expression pattern, the spatial gradient of AN3 protein along the
172 longitudinal axis of leaf primordia did not change. Therefore, the influence of PATI treatment
173 on the AN3 protein accumulation pattern is rather limited.

174 On the other hand, when *an3-4/pAtAN3::AN3-3xGFP* were treated with PATI, we
175 recognized that *AN3* localization was missing in the vasculature region. This missing
176 localization was also observed in control conditions, but in PATI-treated leaves, the vasculature
177 was very thick, and therefore, the absence was recognizable (**Figs. 1D-F**, **4**).
178

179 Cell division angles in leaves

180 To understand how PATI treatment caused the changes in size or pattern of the cell
181 proliferation zone and the leaf shape, analysis of cell division angles was performed using the
182 *gl1-s92f* mutant and *gl1-s92f/an3-4* double mutants. We chose *gl1-s92f* mutants that lacked
183 trichomes as a control WT because trichomes obstruct cell division plane observation using
184 aniline blue staining (**Fig. S1**). The angles were determined against the proximal-distal axis,
185 starting from the leaf base and parallel to the midvein for the first and second rosette leaves of
186 7 DAS seedlings (**Fig. 5**). As a result, a variation in cell division angle patterns was observed
187 (**Fig. 5A**). In the control WT plants, the cell division angle peaked at around 130°–140° (**Fig.**
188 **5A**). In PATI-treated leaves, this peak was less evident, and cell division was likely randomized
189 (**Fig. 5A**). This may have contributed to changes in leaf shape, with rounder and shorter leaves,
190 when treated with PATI (**Figs. 1D-F, 2A**).

191 We performed a cell division angle investigation also for the *an3-4* mutant plants. In
192 the *an3-4* mutant without PATI, the peak of cell division angle was around 140–150°, which
193 differed from that of the WT (**Fig. 5A, B**), suggesting that AN3 might shift the cell division
194 angle to smaller angles, i.e., a shift from proximo-distal to mediolateral direction. This angle
195 shift can explain why the *an3* leaves are narrower than WT leaves. In the *an3* mutant treated
196 with PATI, however, the distribution of cell division angle became similar to that of WT plants
197 treated with PATI (**Fig. 5A, B**), indicating that the randomizing effect of PATI on cell division
198 angle is superior to the effect of the *an3* mutation biasing cell division angle to the proximo-
199 distal axis. In both WT and *an3*, the effects of PATI on the cell division angle seem to be similar
200 between TIBA and NPA, but slightly stronger in NPA than TIBA (**Fig. 5A, B**).

201

202 The position of cell proliferative area in floral organs

203 Then, we examined floral organs as modified leaves. Although floral organs such as
204 sepals, petals, stamens, and carpels are homeotic to leaves, their shapes are different. Even
205 between sepals and petals, both of which are planar organs, there are distinct differences in
206 shape in *A. thaliana*. For example, in the distal part, the sepal is narrower, and the petal is wider,
207 while foliage leaves are narrower in the distal part, similar to sepals.

208 We observed cell proliferation patterns in planar floral organ primordia to investigate
209 whether these patterns might influence the difference in the final organ shape. To visualize
210 dividing cells in floral organs, we used EdU. In a sepal primordium, cell division was observed
211 in the basal part of the organ primordia through the observed developmental stages (**Fig. 6**).
212 The position of cell proliferative area was similar to that of leaf primordium investigated in
213 previous studies (e.g., Donnelly et al., 1999, Kawade et al., 2017) (**Fig. 1**). In contrast, cell
214 division in the petal primordia was observed in the whole organ when the organ was around
215 100–150 μm in length and the distal and marginal regions when the organ was around 400 μm
216 in length **(Fig. 6**), which marked a clear difference from that of leaves and sepals.

217

218 AN3 protein localization in floral organs

219 As AN3 is a key regulator of the leaf meristem position, we suspected that AN3 protein
220 accumulation patterns may be different between leaves and planar floral organs, which have
221 different positions of the cell proliferative area. AN3-GFP signals were only observed in the
222 basal part of sepal organ primordia, whereas the signals were observed in the entire petal organ
223 primordia at first, and then in the distal region in later stages. Moreover, in the petal primordia,
224 sparse signals were also observed in the central region and the basal part in the later stage 9
225 (**Fig. 6**), where EdU signals were rarely observed.

226

227 Phenotype of *an3* mutant in sepal

228 It is reported that *an3* mutants have narrower petals and a smaller number of cells than
229 that of the Col-0 wild type (WT) (Horiguchi et al., 2005; Lee et al., 2009), but the sepal
230 phenotype has not been investigated. The above-mentioned similarity in the AN3 protein
231 accumulation pattern and proliferative area in the sepal primordia strongly suggested that the
232 *AN3* is also involved in meristematic regulation in the sepal. In order to investigate whether
233 AN3 is involved in meristematic regulation as in leaf meristem in sepal primordia, we
234 compared the phenotype of *an3-4* and the WT in the sepals (**Fig. 7A, B**). The area of the organ

235 was smaller in *an3* than in the WT (**Fig. 7C**). We also observed that the *an3* mutant had fewer
236 complex veins as compared to that of the WT, which was evaluated based on the number of
237 secondary and higher veins in the m-shaped or two n-shaped primary veins (**Fig. 7D, E**).
238
239 Cell division angles in floral organs
240 To know the possible contribution of biased cell division angle on the final shape of
241 floral organs, cell division angle analysis was conducted in the sepals and petals from flowers
242 at stages 8–10 where active cell proliferation is known (Alvarez-Buylla et al., 2010). The
243 distribution pattern of cell division angle in planar floral organs was unique in showing loose
244 double peaks (**Fig. 8A**) that is different from the cell division angle in leaves, which had one
245 peak (**Fig. 5A, B**). Irrespective of the similarity between sepals and leaves in terms of
246 localization of the cell proliferation zone, the overall tendency of cell division in sepals was
247 similar to that of petals. This suggests that the pattern of cell division angles is not associated
248 with the localization of the cell proliferation zone but with organ identity.
249 To understand further the unique cell division patterns in these floral organs, we also
250 analyzed the spatial distribution of the cell division angles in the primordia (**Fig. 8B**). As a
251 result of the sepal primordia, the cell divisions within the 60°–90° range, which were divisions
252 in the mediolateral direction of the primordia, were identified more distally than the divisions
253 that corresponded to the 140°–180° range, which were divisions in the proximo-distal direction
254 (**Fig. 8B**), which may contribute to the oval-shaped sepal primordia. On the other hand, in the
255 petals, the cell divisions within the 60°–90° range, which were divisions in the mediolateral
256 direction of the primordia, were identified mostly in the central regions of the petal primordia.
257 The divisions that corresponded to the 140°–180° range were identified mostly in the marginal
258 regions of the petal primordia (**Fig. 8B**).
259
260 **Discussion**
261 In this study, we examined how cell proliferative zones differ in the primordia of PATI-
262 treated leaves and floral organs from normal foliage leaf primordia of *A. thaliana* with a focus
263 on the spatial expression pattern of *AN3*, a key element for leaf meristem positioning (Kawade
264 et al., 2010). We identified that organ shape variation by PATI treatment cannot be attributed
265 to changes in leaf-meristem positioning, size of the leaf meristem, or the expression pattern of
266 *AN3* but is rather attributed to altered cell division angles in the leaf meristem. Interestingly,
267 the *an3* mutation biased cell division angle to the proximo-distal axis in the leaf meristem,
268 whereas PATI treatment randomized the angle. These effects on the cell division angle are

269 reasonable considering that the *an3* has narrower leaves and PATI-treated leaves are shorter
270 and rounder (**Figs. 1, 2, 4**). Because polar auxin flow is highly plausible to polarize the cell
271 division angle (Yin and Tsukaya 2016; reviewed in Dhonukshe et al. 2005), the observed
272 phenomena could be explained as follows: AN3 randomized the cell division angle (or shift
273 the angle from proximo-distal to mediolateral direction) against the auxin-dependent polarity;
274 PATI randomized the cell division angle by cancelling the auxin flow. Since along the
275 vasculatures *AN3* mRNA expression was not observed (**Fig. 1D-F**), polarized cell division
276 angle along the vasculature in the WT (Yin and Tsukaya 2016) could be explained by the
277 absence of AN3.
278 Different shapes of sepals and petals compared with foliage leaves were found to be
279 correlated with both altered meristem position associated with altered *AN3* spatial expression
280 patterns and different distributions of cell division angles. Overall, our results strongly suggest
281 that lateral organ shapes are regulated via two aspects: position of meristem and cell division
282 angles; the former is mainly governed by the *AN3* expression pattern. In the following sections,
283 several aspects of the above findings are discussed.
284
285 <u>The position of leaf meristem in PATI-treated plants</u>
286 When *A. thaliana* plants were treated with PATI, both the cell proliferation zone and
287 *AN3*-expression zone still sit in the proximal par of leaf primordia. It was also observed that
288 under the PATI treatment the *AN3* mRNA expression zone was slightly expanded to the distal
289 direction in the expression zone ratio, although the final AN3 protein distribution remained
290 unchanged (**Fig. 4M, N**). As previously reported (Sieburth, 1999) and confirmed here (**Figs. 1-**
291 **3**), PATI-treated leaves were rounder and shorter, whereas a longer proliferation zone would
292 be expected to produce a longer leaf if the other aspects were not changed. Instead, we found
293 that changes in the cell division angles could be attributed to the altered leaf shape.
294 We also observed that the *AN3* promoter was not expressed in leaf veins (**Fig. 4A-L**).
295 This trend was clearly seen in PATI-treated leaves as well as in control conditions; however, it
296 was not evident in control conditions because the veins were much thinner than those of PATI-
297 treated leaves (**Fig. 1D-F**). This may happen if *AN3* expression is shut down in differentiated
298 vascular cells, which may imply that the vasculature differentiation by auxin is superior to cell
299 proliferation maintenance by AN3.
300

301 Cell division angle and leaf shape

302 Cell division is an important factor in both leaf development and leaf vein architecture
303 (Kang et al., 2007). In this study, analysis of the cell division angle revealed that the pattern
304 differed between PATI-treated plants and control plants (**Fig. 5A**). This difference in the pattern
305 could be a cause for the differences in leaf shape. In comparison with control leaf primordia
306 that had major division angles in 130°–140°, PATI-treated leaf primordia had dispersed
307 division angles in many directions, forming a round and short leaf, which matched the
308 phenotype (**Figs. 1D-F**, **3**). This suggests that auxin flow regulates leaf shape via controlling
309 cell division orientation in the leaf meristem. It has been shown that the presence of
310 vasculatures is important in determining cell division patterns (Yin and Tsukaya, 2016).
311 Therefore, the thickened midveins, where many veins running in the same direction along
312 proximal-distal axis observed in PATI-treated leaves, may have indirectly affected the cell
313 division angle.
314

315 Determining cell division angle in leaves

316 In this study, two components changed the cell division angle: PAT and AN3. When
317 PAT was inhibited, the peak in the cell division angle distribution became less evident (**Fig.**
318 **5A**). As auxin flow controls vascular cell polarity (Linh et al., 2018) it is possible that the cells
319 divide in the direction of auxin flow. In addition, both NPA and TIBA affect actin dynamics
320 (Teale and Palme, 2018; Zou et al., 2019) that can affect cytoskeletal regulation of cytokinesis,
321 and may be one of the underlying reasons for the change in cell division angle.

322 We observed the *an3* mutant tended to divide around 140°–150°, which partially
323 explains the narrow leaf phenotype of *an3* mutants, as cell division along the proximal-distal
324 axis was increased (**Fig. 5B**). In a previous report, the phase of cell division was divided into
325 two phases: the first has more divisions along the proximal-distal axis than the second phase
326 (Horiguchi et al., 2011). In the latter phase, except for marginal area and local areas along veins
327 cell division orientation was randomized (Yin and Tsukaya 2016). Furthermore, in *an3* mutants,
328 the transition from the first to the second phase does not occur before the termination of cell
329 division activity (Horiguchi et al., 2011). The shift in the peak of the cell division angle
330 observed in the *an3* mutant would reflect this failure in shifting to the second phase of cell
331 proliferation, which confirms the results of previous studies. Therefore, AN3 functions in the
332 transition to the second phase of cell division, and consequently, cells tend to divide along the
333 proximal-distal axis in the absence of AN3. Precisely, AN3 might promote the shift of the cell
334 division angle from the proximo-distal preference to the randomized one.

335 In addition, in *an3* mutants treated with PATI, the cell division angles were similar to
336 those of WT treated with PATI (**Fig. 5A, B**). This suggests that the randomizing effect of PATI
337 on cell division angle is superior to that of AN3 and that the loss of PAT results in cell division
338 in random directions irrespective of the presence or absence of AN3. This might be explained
339 as follows: AN3 functions for the phase shift from proximo-distal preference to randomized
340 one; polar auxin transport is directly or indirectly involved in the polar-dependent cell division
341 angle in both phases; loss of AN3 activity and PAT results in more proximo-distal and
342 randomized cell division, respectively. If the PAT-dependent polarity axis is lost, even in the
343 *an3*, the cell division angle is randomized.
344
345 Position of meristematic tissue determines the final floral organ shape
346 The final organ shape could be determined by various factors, such as acceleration
347 and deceleration of proliferation, oriented cell division and expansion, and the meristem
348 position (Tsukaya, 2018). In this study, we showed that the position of the cell proliferative
349 area was completely different between sepals and petals, which are both modified leaves but
350 morphologically different. The petal of *A. thaliana* with a modest fan shape has a proliferative
351 region in the distal part, which is similar to ferns with fan-shaped morphology, which is rare in
352 angiosperm leaves, coinciding with leaf meristem at the apical margin (Boyce, 2007; Tsukaya,
353 2014, 2018). This suggests that the morphological differences between sepals and petals could
354 be at least partly explained by the meristematic position in each organ.
355 Although predominant cell division occurs in submarginal plate meristem to widen
356 the leaf blade area in leaf primordia (e.g., Poethig and Sussex, 1985), it was also shown that
357 marginal meristem residing in the margin of the primordia is present (Alvarez et al., 2016;
358 reviewed in Tsukaya 2021). Alvarez et al. (2016) showed that when NGATHA and
359 CINCINNATA-class-TCP were knocked down, indeterminate marginal growth occurred in the
360 entire margin of the leaf blade, suggesting potential meristem activity in this area. Interestingly,
361 marginal growth occurs only in the distal region of floral organs in their system, including
362 sepals and petals. In terms of WT petals, active cell division occurs in the distal margin in the
363 first place (Sauret-Güeto et al. 2013; our present study, **Fig. 6**); therefore, the marginal
364 meristem may contribute more than leaves or sepals. Since the activity of meristem in the distal
365 marginal area of a blade has been discussed as an ancestral character (Floyd and Bowman,
366 2010), petals may retain this developmental character (Boyce, 2007). We observed EdU signals
367 in the entire margin of the petal primordia at least until the organ size was 400 μm in length,
368 even in the proximal region. Considering the results of Alvarez et al. (2016) on leaf and floral

369 organ primordia, the nature of proliferative cells in marginal areas is different among different
370 lateral organs.
371
372 Role of AN3 in planar lateral organs
373 Several key genes are known to positively control cell proliferation in the leaf
374 meristem (Nakata et al., 2012; Ichihashi and Tsukaya, 2015; Tsukaya, 2021). Among them, the
375 AN3-protein-accumulated region matches with the cell proliferative area in leaf primordia
376 (Kawade et al., 2017), suggesting that AN3 is an important determinant of the leaf meristem
377 position. Moreover, the smaller size of a petal in *an3* or triple knockdown of the GIF family
378 (Kim and Kende, 2004; Horiguchi et al., 2005; Lee et al., 2009) suggested that AN3 is also
379 involved in the promotion of cell proliferation in the petal. However, its functioning zone in
380 primordia has not been well investigated. In this study, we showed that the AN3-expressed
381 region overlapped with the cell proliferative area in both sepals and petals, as observed in leaf
382 primordia. In addition, we first showed that traits of sepals in *an3* mutants are likely to have
383 fewer cells as petals or foliage leaves. These results suggest that AN3 functions as a
384 determinant of the meristematic position and activity in all planar floral organs. However, in
385 terms of petal primordia, AN3 protein signals were also observed in the less proliferative area.
386 This might be due to a lack of associating transcriptional factors such as GROWTH
387 REGULATING FACTOR5 (GRF5), which is necessary to promote cell proliferation in leaf
388 primordia (Horiguchi et al., 2005), in such regions. Alternatively, because signals in the
389 proximal part were not as strong as those in the distal region, the concentration of AN3 proteins
390 might not be enough to promote cell division to the extent that EdU was incorporated.
391 In the past, JAGGED (JAG) was examined as a candidate of a regulatory gene for the
392 specific morphology in the *Arabidopsis* petal that differed from leaves because the loss-of-
393 function *jag* mutant has narrower and shorter petals; the *JAG* overexpressor has larger petals;
394 its mRNA is expressed distal margin (Sauret-Güeto et al. 2013). At that time point, JAG was
395 the only candidate 'organizer' that presented the petal with a pattern of growth orientations that
396 fans out. However, AN3 has become an additional candidate that fulfills the required, above-
397 mentioned conditions. Indeed, *AN3* was identified as a direct target of JAG (Schiessl et al.
398 2014). The role of AN3 as the 'organizer' sensu Sauret-Güeto et al. (2013) should be examined
399 in the future.
400 To fully understand the mechanisms of flower organogenesis, the regulation of
401 meristem position by floral organ identity genes needs to be investigated (Coen and

402 Meyerowitz, 1991). Honma and Goto (2001) and Pelaz et al. (2001) revealed that when A genes
403 (*APELATA1*) and B genes (*APELATA3* and *PISTILATA*) were ectopically expressed together
404 with *SEPALLATA2/3* in rosette leaves, the rosette leaves obtained petal identity, and the color
405 and cell shape became petal-like. However, the transformed petaloid organ was not fan-shaped
406 but had a taper off shape, which was similar to rosette leaves, cauline leaves, and sepals. This
407 suggests that factors other than the floral identity homeotic genes control the final organ shape.
408 Revealing the mechanisms of *AN3* expression control might shed light on which factors are
409 involved in the resulted different morphology among different organs.

410 The leaves of some gymnosperms and ferns are considered to grow from the
411 meristem in the distal margin. The positioning of these meristems may also be determined by
412 the spatial distribution of leaf meristem-controlling genes, such as *AN3/GIF1*. As *GIF* family
413 genes exist in most eukaryotic organisms, including the basal land plants, *Marchantia*
414 *polymoprha*, *Physcomitrium patens*, and *Sellaginella moellendorffi* (Kim and Tsukaya, 2015),
415 further analyses of the *GIFs* in gymnosperms and ferns could answer this question.
416

417 <u>Determining cell division angle in floral organs</u>

418 In this study, the cell division pattern in floral organ primordia was investigated for its
419 possible roles in each floral organ morphology. Both the petals and sepals showed a pattern
420 with loose twin peaks in the distribution of cell division angles, which was different from that
421 of leaf primordia that had a clear single peak (**Fig. 6**). This is an interesting new finding on the
422 meristems in these primordia. In addition, we found that in the petal the cell division occurred
423 at 60°–90° angle in the central regions, and the cell division with the 140°–180° angle was
424 mostly in the marginal regions, whereas such a pattern was not seen in the sepals (instead
425 longitudinal distribution was observed, **Fig. 8**). This difference may cause variation in shape
426 between sepals and petals, with the distal part being wider than the proximal part, which may
427 be caused by the cell divisions that contributed to width in the marginal regions. Although both
428 sepal and leaf primordia have a cell proliferation zone in the basal region, the cell division
429 angle was controlled differently, which may imply that cell division angles depend on organ
430 identity and affect their final shapes.

431 Overall, our results imply that lateral organ shapes are likely to be regulated by two
432 factors: the position of the cell proliferative zone governed by the spatial expression pattern of
433 *AN3* and cell division angles. Therefore, even in one species, by changing these two factors, a

434 variety of lateral organ shapes could be performed. To test this idea, future studies with a
435 combination of genetic manipulation and computer simulation should be carried out.
436
437 **Materials and Methods**
438 Plant growth
439 For analysis of the leaf primordia, *A. thaliana* Col-0 (WT), or those carrying
440 *CYCLINB1;1*(*CYCB1;1*)::GUS, *an3-4*, *an3-4*/*pAtAN3::AN3-GFP*, *an3-4*/*pAtAN3::AN3-*
441 *3xGFP*, *gl-s92f*, or *gl-s92f*/*an3* were grown on sterile growth medium that contained half-
442 strength Murashige and Skoog medium (MS, Wako, Osaka, Japan), 1% (w/v) sucrose (Nacalai
443 Tesque, Kyoto, Japan), and 0.8% (w/v) agar (Nacalai Tesque, Kyoto, Japan) (Wako, Osaka,
444 Japan) adjusted to pH 5.8 with potassium hydroxide. Approximately, 1 M PATI (TIBA and
445 NPA) stocks were dissolved in dimethyl sulfoxide and added to the medium to a final
446 concentration of 10 μM. The medium composition was based on that described by Sieburth
447 (1999).
448 Seeds were sterilized by immersing in a solution of 2% (v/v) Plant Preservative
449 Mixture™ (Plant Cell Technology, Washington, D.C., USA), 0.1% (v/v) Triton X-100 (Nacalai
450 Tesque, Kyoto, Japan), and 50 mg/L $MgSO_4$ for 6 h or a solution of 10% (v/v) sodium
451 hypochlorite (Nacalai Tesque, Kyoto, Japan) and 1% (v/v) Triton X-100 for 5 min and twice
452 with sterile water prior to plating. The plates were incubated at 24°C under constant
453 illumination.
454 For analyses of the floral organ primordia, *A. thaliana* Col-0 and *an3-4*/*pAtAN3::AN3-*
455 *1xGFP* (Kawade et al., 2013) were sown on rockwool (Toyobo, Osaka, Japan) and grown under
456 white fluorescent light conditions (ca. 40 μmol m^{-2} s^{-1}) at 22–23°C supplied with water
457 containing 1 g/L powder Hyponex (Hyponex, Osaka, Japan).
458
459 GUS experiments
460 Detection of GUS activity was carried out using 5-bromo-4-chloro-3-indolyl-β-D-
461 glucuronide (X-Gluc) as a substrate. Plant tissue was first placed in 90% (v/v) acetone on ice
462 for 10 min, washed with sodium phosphate buffer (pH 7.0), and then placed in X-Gluc buffer
463 solution (0.5 mg/mL X-Gluc, 100 mM $NaPO_4$ (pH 7.0), 5 mM $K_3Fe(CN)_6$, 5 mM $K_4Fe(CN)_6$,
464 10 mM EDTA, 0.1% (v/v) Triton X-100) under vacuum for 15 min or more and then placed in
465 the dark at room temperature (ca. 20°C).
466 After GUS detection, plant tissues were rinsed in 70% (v/v) ethanol and fixed in
467 ethanol: acetic acid (6:1) solution. After chlorophyll was removed, the tissue was preserved in

468 70% EtOH in the dark. Plant tissues were mounted on slides with chloral hydrate solution (50
469 g chloral hydrate, 5 g glycerol, 12.5 mL distilled water) (Tsuge et al., 1996) and observed under
470 a microscope after the tissue became transparent enough.
471
472 AN3-GFP observations
473 Leaf primordia (5 DAS) and flower primordia of *A. thaliana an3-4/pAN3::AN3-GFP*
474 and *an3-4/pAN3::AN3-3xGFP* lines were fixed in 4% (v/v) paraformaldehyde (PFA) in
475 phosphate-buffered saline (PBS) with 0.05% (v/v) Triton X-100 by immersing them in the
476 fixation mixture, deairing them for 10 min (for leaf primordia) or 15 min (twice, for flower
477 primordia) and placed at 4°C overnight. The samples were then washed in PBS (10 min, twice)
478 and stored in PBS at room temperature for leaf primordia and 4°C for flower primordia until
479 observation.
480 The samples were then dissected using a sharp razor under the microscope. Leaf
481 primordia were mounted on slides with PBS and observed under a confocal microscope
482 (FV3000; Olympus, Tokyo, Japan) with a GFP filter for leaf primordia and an upright
483 fluorescent microscope (DM4000; Leica Microsystems GmbH, Wetzlar, Germany) for floral
484 organ primordia.
485
486 Data analysis on the area of cell proliferative area and AN3-GFP localized area
487 We used a method derived from Kazama et al. (2010) and Ikeuchi et al. (2011) to
488 determine the position of leaf meristem. First, an image of a leaf with a GUS expression pattern
489 was prepared. The outer region of the leaf was cropped, and the image was rotated so that the
490 leaf base was on the left side of the image. Then, the blue region was extracted, and a binary
491 image was created using ImageJ (https://imagej.nih.gov/ij/). The number of white pixels was
492 counted for each column, and the end of the cell proliferative area along the proximal-distal
493 axis (hereafter referred to as arrest front) was determined based on the definition of the point
494 at which the ratio of white pixels was half that of the maximum and farthest from the blade
495 base. The distance from the leaf base of each arrest front point was plotted for each condition
496 in a box plot. Statistical analysis was performed using the R software.
497 Similarly, AN3-GFP localized area was determined as follows: first, a series of z-stack
498 images were stacked using ImageJ software. Stacked images with the outer side of the leaf
499 were cropped and rotated so that the leaf base was on the left side of the image. The region
500 with AN3-GFP fluorescence was extracted, and from this image, a binary image was created.
501 The number of black pixels was counted in each column. The end of the AN3-GFP localized

area was determined based on the definition of the point at which the ratio of black pixels was half that of the maximum and farthest from the blade base. The distance from the leaf base of each end of the AN3-GFP localized area was divided by the leaf length because of the size difference between lines. The obtained data were plotted for each condition in a box plot. Statistical analysis was performed using the R software.

Observation of Aniline Blue signal

We used a method derived from previous studies for the detection of newly formed cell walls (Kuwabara and Nagata, 2006; Kuwabara et al., 2011). Leaf primordia (7 DAS) of *A. thaliana glabra1(gl1)-s92f* and *gl1-s92f/an3-4* mutants and Col-0 flower petals and sepals were first fixed in a mixture of ethanol and acetic acid (4:1, v/v) for 30 min and then rinsed in 100% ethanol. Then, the samples were immersed in a mixture of ethanol and 100 mM phosphate buffer (pH 9.0; 1:1, v/v) for 30 min and then in 100 mM phosphate buffer (pH 9.0) for 10 min. Finally, the samples were immersed in a 0.02% (w/v) solution of aniline blue in 100 mM phosphate buffer (pH 9.0) for at least 7 days and up to 30 days at 4°C. Leaf primordia were mounted on slides with the staining solution and observed under a confocal microscope (FV10C-PSU; Olympus, Tokyo, Japan) under UV excitation with a DAPI (4',6-diamidino-2-phenylindole) filter. The data were analyzed by taking each angle of the septum wall. Calculations were performed using Microsoft® Excel.

Observation of EdU-marked cells

We used the Click-iT EdU Alexa Fluor 488 Imaging Kit (Thermo Fischer Scientific, Waltham, MA, USA) to visualize the cells in S phase. We dissected the inflorescence of *A. thaliana* into several pieces and soaked the flower clusters into 10 μM 5-ethynyl-2'-deoxyuridine (EdU) solution in half-strength MS medium with 1% sucrose for 3 h under ~45 μmol m^{-2} s^{-1} white fluorescent light. The samples were washed with PBS containing 0.1% Triton X-100 and fixed with FAA (37% [v/v] formaldehyde, 5% [v/v] acetic acid, 50% [v/v] ethanol) and stored at 4°C. Subsequent fluorescent labeling with Alexa Fluor 488 or 555 (Thermo Fischer Scientific, Waltman, MA, USA) was conducted according to the manufacturer's instructions. Floral organs were mounted on slides, and fluorescent dye signals conjugated to EdU were observed under fluorescent microscope (DM4000; Leica Microsystems GmbH, Wetzlar, Germany).

Acknowledgments

We would like to thank MEXT and the Graduate Program for Leaders in Life Innovation (GPLLI)/World-leading Innovative Graduate Study Program for Life Science and Technology (WINGS-LST) of the University of Tokyo for providing microscope facilities.

Author Contributions

AK, MN, and HT designed the experiments; AK and MN performed the experiments and analyzed the data; AK, MN, and HT wrote the manuscript.

Funding

This research was supported by a Grant-in-Aid for JSPS Fellows (AK, #19J14140) and a Grant-in-Aid for Scientific Research on Innovation Areas (HT, #25113002 and 19H05672) from MEXT and GPLLI/WINGS-LST of the University of Tokyo (AK).

Conflict of Interest

No conflict of interest.

Data Availability

Data is available on request from the authors.

555

556 **References**

557 **Alvarez-Buylla ER, Benítez M, Corvera-Poiré A, Chaos Cador Á, de Folter S, Gamboa**
558 **de Buen A, Garay-Arroyo A, García-Ponce B, Jaimes-Miranda F, Pérez-Ruiz R V.,** et
559 al**. 2010**. Flower Development. *The Arabidopsis Book* **8**: e0127.

560 **Alvarez JP, Furumizu C, Efroni I, Eshed Y, Bowman JL**. **2016**. Active suppression of a
561 leaf meristem orchestrates determinate leaf growth. *eLife* **5**: e15023.

562 **Anastasiou E, Kenz S, Gerstung M, MacLean D, Timmer J, Fleck C, Lenhard M**. **2007**.
563 Control of plant organ size by KLUH/CYP78A5-dependent intercellular signaling.
564 *Developmental Cell* **13**: 843–856.

565 **Boyce CK**. **2007**. Mechanisms of laminar growth in morphologically convergent leaves and
566 flower petals. *International Journal of Plant Sciences* **168**: 1151–1156.

567 **Candela H, Martínez-Laborda A, Luis Micol J**. **1999**. Venation pattern formation in
568 *Arabidopsis thaliana* vegetative leaves. *Developmental Biology* **205**: 205–216.

569 **Cheng Y, Dai X, Zhao Y**. **2006**. Auxin biosynthesis by the YUCCA flavin monooxygenases
570 controls the formation of floral organs and vascular tissues in Arabidopsis. *Genes and*
571 *Development* **20**: 1790–1799.

572 **Coen ES, Meyerowitz EM**. **1991**. The war of the whorls: genetic interactions controlling
573 flower development. *Nature* **353**: 31–37.

574 **Dengler N, Kang J**. **2001**. Vascular patterning and leaf shape. *Current Opinion in Plant*
575 *Biology* **4**: 50–56.

576 **Dinneny JR, Yadegari R, Fischer RL, Yanofsky MF, Weigel D. 2004**. The role of
577 JAGGED in shaping lateral organs. *Development* **131**: 1101-1110. doi:10.1242/dev.00949

578 **Dhonukshe P, Kleine-Vehn J, Friml J. 2005.** Cell polarity, auxin transport, and
579 cytoskeleton-mediated division planes: who comes first? *Protoplasma* **226**: 67-73.

580 **Disch S, Anastasiou E, Sharma VK, Laux T, Fletcher JC, Lenhard M**. **2006**. The E3
581 ubiquitin ligase BIG BROTHER controls Arabidopsis organ size in a dosage-dependent
582 manner. *Current Biology* **16**: 272–279.

583 **Donnelly PM, Bonetta D, Tsukaya H, Dengler RE, Dengler NG**. **1999**. Cell cycling and
584 cell enlargement in developing leaves of *Arabidopsis*. *Developmental Biology* **215**: 407–419.

585 **Esau K**. **1977**. *Anatomy of Seed Plants, 2nd Edition*. New York: John Wiley & Sons.

586 **Floyd SK, Bowman JL**. **2010**. Gene expression patterns in seed plant shoot meristems and
587 leaves: Homoplasy or homology? *Journal of Plant Research* **123**: 43–55.

588 **Honma T, Goto K. 2001.** Complexes of MADS-box proteins are sufficient to convert leaves
589 into floral organs. *Nature* **409**: 524–529.
590 **Horiguchi G, Kim GT, Tsukaya H**. **2005**. The transcription factor AtGRF5 and the
591 transcription coactivator AN3 regulate cell proliferation in leaf primordia of *Arabidopsis*
592 *thaliana*. *Plant Journal* **43**: 68–78.
593 **Horiguchi G, Nakayama H, Ishikawa N, Kubo M, Demura T, Fukuda H, Tsukaya H**.
594 **2011**. *ANGUSTIFOLIA3* plays roles in adaxial/abaxial patterning and growth in leaf
595 morphogenesis. *Plant and Cell Physiology* **52**: 112–124.
596 **Ichihashi Y, Kawade K, Usami T, Horiguchi G, Takahashi T, Tsukaya H**. **2011**. Key
597 proliferative activity in the junction between the leaf blade and leaf petiole of Arabidopsis.
598 *Plant Physiology* **157**: 1151–1162.
599 **Ichihashi Y, Tsukaya H**. **2015**. Behavior of leaf meristems and their modification. *Frontiers*
600 *in Plant Science* **6**: 1–8.
601 **Ikeuchi M, Yamaguchi T, Kazama T, Ito T, Horiguchi G, Tsukaya H**. **2011**.
602 ROTUNDIFOLIA4 regulates cell proliferation along the body axis in arabidopsis shoot.
603 *Plant and Cell Physiology* **52**: 59–69.
604 **Kang J, Mizukami Y, Wang H, Fowke L, Dengler NG**. **2007**. Modification of cell
605 proliferation patterns alters leaf vein architecture in Arabidopsis thaliana. *Planta* **226**: 1207–
606 1218.
607 **Kawade K, Horiguchi G, Tsukaya H**. **2010**. Non-cell-autonomously coordinated organ size
608 regulation in leaf development. *Development* **137**: 4221–4227.
609 **Kawade K, Horiguchi G, Usami T, Hirai MY, Tsukaya H**. **2013**. ANGUSTIFOLIA3
610 signaling coordinates proliferation between clonally distinct cells in leaves. *Current Biology*
611 **23**: 788–792.
612 **Kawade K, Tanimoto H, Horiguchi G, Tsukaya H**. **2017**. Spatially different tissue-scale
613 diffusivity shapes ANGUSTIFOLIA3 gradient in growing leaves. *Biophysical Journal* **113**:
614 1109–1120.
615 **Kazama T, Ichihashi Y, Murata S, Tsukaya H**. **2010**. The mechanism of cell cycle arrest
616 front progression explained by a *KLUH/CYP78A5*-dependent mobile growth factor in
617 developing leaves of *Arabidopsis thaliana*. *Plant and Cell Physiology* **51**: 1046–1054.
618 **Kim JH, Kende H**. **2004**. A transcriptional coactivator, AtGIF1, is involved in regulating
619 leaf growth and morphology in *Arabidopsis*. *Proceedings of the National Academy of*
620 *Sciences of the United States of America* **101**: 13374–13379.

621 **Kim, JH. and Tsukaya, H.** (2015). Regulation of plant growth and development by the
622 GROWTH-REGULATING FACTOR and GRF-INTERACTING FACTOR duo. *Journal of*
623 *Experimental Botany* **66**, 6093–6107.**Kuwabara A, Backhaus A, Malinowski R, Bauch M,**
624 **Hunt L, Nagata T, Monk N, Sanguinetti G, Fleming A**. **2011**. A shift toward smaller cell
625 size via manipulation of cell cycle gene expression acts to smoothen arabidopsis Leaf Shape.
626 *Plant Physiology* **224**: 761–770.
627 **Kuwabara A, Nagata T**. **2006**. Cellular basis of developmental plasticity observed in
628 heterophyllous leaf formation of Ludwigia arcuata (Onagraceae). *Planta* **224**: 761–770.
629 **Lee BH, Ko JH, Lee S, Lee Y, Pak JH, Kim JH**. **2009**. The Arabidopsis *GRF-*
630 *INTERACTING FACTOR* gene family performs an overlapping function in determining
631 organ size as well as multiple developmental properties. *Plant Physiology* **151**: 655–668.
632 **Lee BH, Wynn AN, Franks RG, Hwang Y sic, Lim J, Kim JH**. **2014**. The arabidopsis
633 thaliana GRF-interacting factor gene family plays an essential role in control of male and
634 female reproductive development. *Developmental Biology* **386**: 12–24.
635 **Linh NM, Verna C, Scarpella E**. **2018**. Coordination of cell polarity and the patterning of
636 leaf vein networks. *Current Opinion in Plant Biology* **41**: 116–124.
637 **Mattsson J, Sung ZR, Berleth T**. **1999**. Responses of plant vascular systems to auxin
638 transport inhibition. *Development* **126**: 2979–2991.
639 **Nakata M, Matsumoto N, Tsugeki R, Rikirsch E, Laux T, Okada K**. **2012**. Roles of the
640 middle domain-specific *WUSCHEL-RELATED HOMEOBOX* genes in early development of
641 leaves in *Arabidopsis*. *Plant Cell* **24**: 519–535.
642 **Nelissen H, Eeckhout D, Demuynck K, Persiau G, Walton A, van Bel M, Vervoort M,**
643 **Candaele J, De Block J, Aesaert S,** et al**. 2015**. Dynamic changes in ANGUSTIFOLIA3
644 complex composition reveal a growth regulatory mechanism in the maize leaf. *Plant Cell* **27**:
645 1605–1619.
646 **Okada K, Ueda J, Komaki MK, Bell CJ, Shimura Y**. **1991**. Requirement of the auxin
647 polar transport system in early stages of *Arabidopsis* floral bud formation. *The Plant Cell* **3**:
648 677–684.
649 **Pelaz S, Gustafson-Brown C, Kohalmi SE, Crosby WL, Yanofsky MF**. **2001**. *APETALA1*
650 and *SEPALLATA3* interact to promote flower development. *The Plant Journal* **26**: 385–394.
651 **Poethig RS, Sussex IM**. **1985**. The cellular parameters of leaf development in tobacco: a
652 clonal analysis. *Planta* **165**: 170–184.

Sauret-Güeto S, Schiessl K, Bangham A, Sablowski R, Coen E. 2013. JAGGED controls Arabidopsis petal growth and shape by interacting with a divergent polarity field. *PLoS Biology* **11**: e1001550. doi:10.1371/journal.pbio.1001550

Sawchuk MG, Edgar A, Scarpella E. **2013**. Patterning of leaf vein networks by convergent auxin transport pathways. *PLoS Genetics* **9**: e1003294.

Schiessl K, Muiñob JM, Sablowski R 2014. Arabidopsis JAGGED links floral organ patterning to tissue growth by repressing Kip-related cell cycle inhibitors. *Proceedings of the National Academy of Sciences of the United States of America* **111**: 2830-2835. www.pnas.org/cgi/doi/10.1073/pnas.1320457111

Sieburth LE. **1999**. Auxin is required for leaf vein pattern in Arabidopsis. *Plant Physiology* **121**: 1179–1190.

Teale W, Palme K. **2018**. Naphthylphthalamic acid and the mechanism of polar auxin transport. *Journal of Experimental Botany* **69**: 303–312.

Tsuge T, Tsukaya H, Uchimiya H. **1996**. Two independent and polarized processes of cell elongation regulate leaf blade expansion in *Arabidopsis thaliana* (L) Heynh. *Development* **122**: 1589–1600.

Tsukaya H. **2014**. Comparative leaf development in angiosperms. *Current Opinion in Plant Biology* **17**: 103–109.

Tsukaya H. **2018**. Leaf shape diversity with an emphasis on leaf contour variation, developmental background, and adaptation. *Seminars in Cell and Developmental Biology* **79**: 48–57.

Tsukaya H. 2021. The leaf meristem enigma: The relationship between the plate meristem and the marginal meristem. *The Plant Cell* doi:10.1093/plcell/koab190

Verna C, Ravichandran SJ, Sawchuk MG, Linh NM, Scarpella E. **2019**. Coordination of tissue cell polarity by auxin transport and signaling. *eLife* **8**: e51061.

Yin X, Tsukaya H. **2016**. A pulse-chase strategy for EdU labelling assay is able to rapidly quantify cell division orientation. *The New phytologist* **211**: 1462–1469.

Zou M, Ren H, Li J. **2019**. An auxin transport inhibitor targets villin-mediated actin dynamics to regulate polar auxin transport. *Plant Physiology* **181**: 161–178.

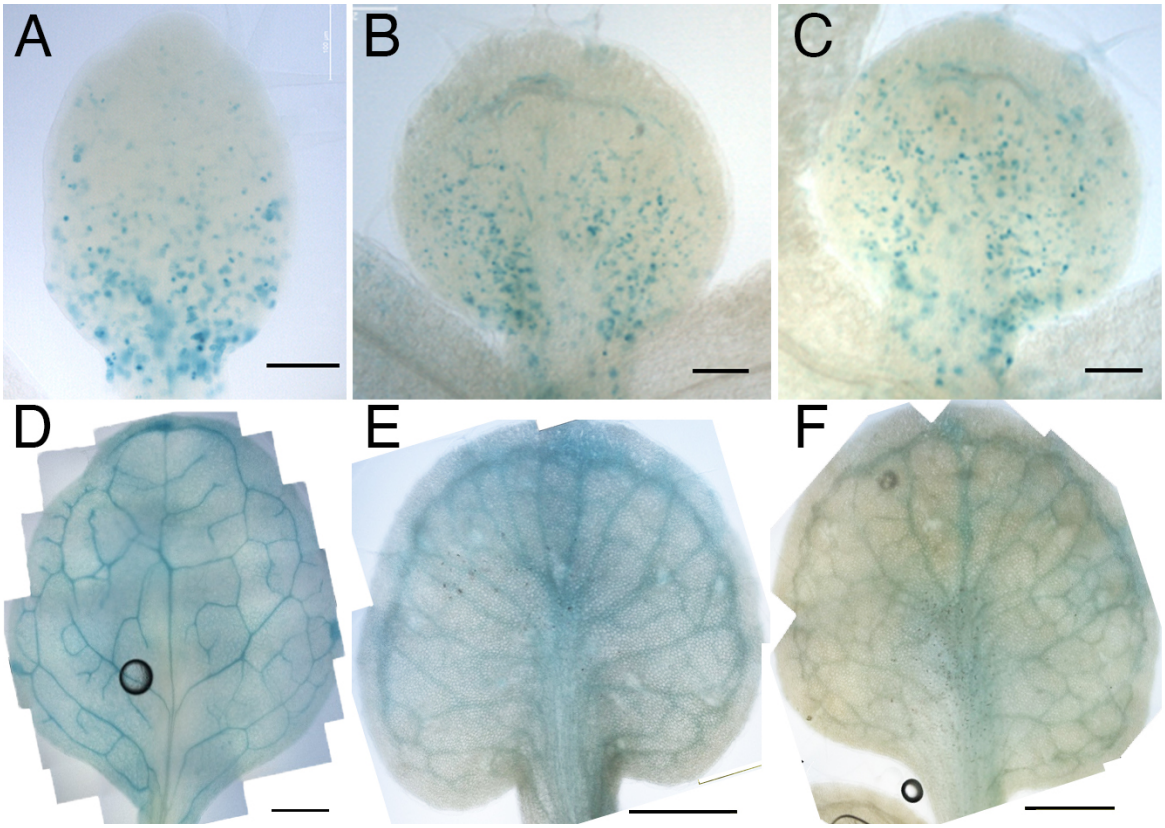

Fig. 1 Cell proliferation is visualized by GUS staining in PATI-treated *CYCB1;1::GUS*.
A: 6 DAS control, B: 7 DAS TIBA-treated, C: 7 DAS NPA-treated leaf primordia.
D: 12 DAS control, E: 12 DAS TIBA-treated, F: 12 DAS NPA-treated leaf primordia. Leaf primordia of similar lengths were compared.
Scale bars: A: 100 µm, B, C: 200 µm, D-F: 500 µm

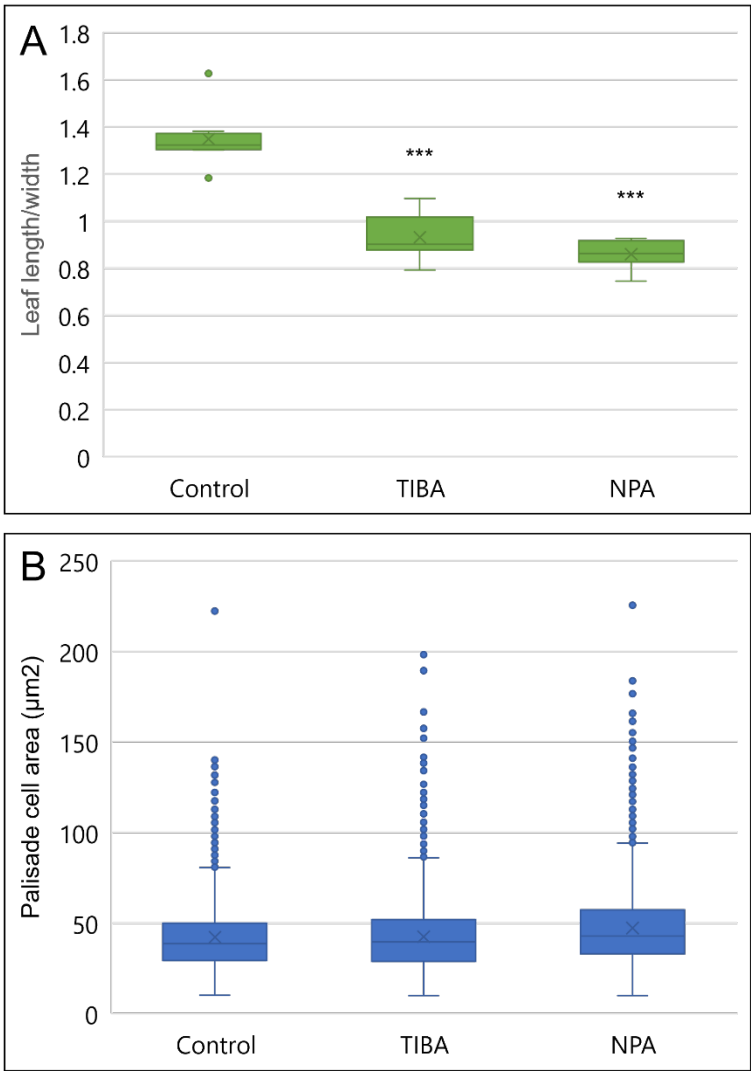

Fig. 2

A: Leaf length/width ratio of leaf primordia at cell proliferation stage. Leaf length was measured after excluding the petiole, as shown in Figure 3A. Leaf width was measured after the leaf has been flattened out on glass slides.

From left to right, data on control (6 DAS), TIBA-treated (7 DAS), and NPA-treated (7 DAS) leaf primordia are shown, n = 4, Dunnett's test ***: $p < 0.001$

B: Palisade cell area for each condition. From left to right, data on control (6 DAS), TIBA-treated (7 DAS), and NPA-treated (7 DAS) n = 4

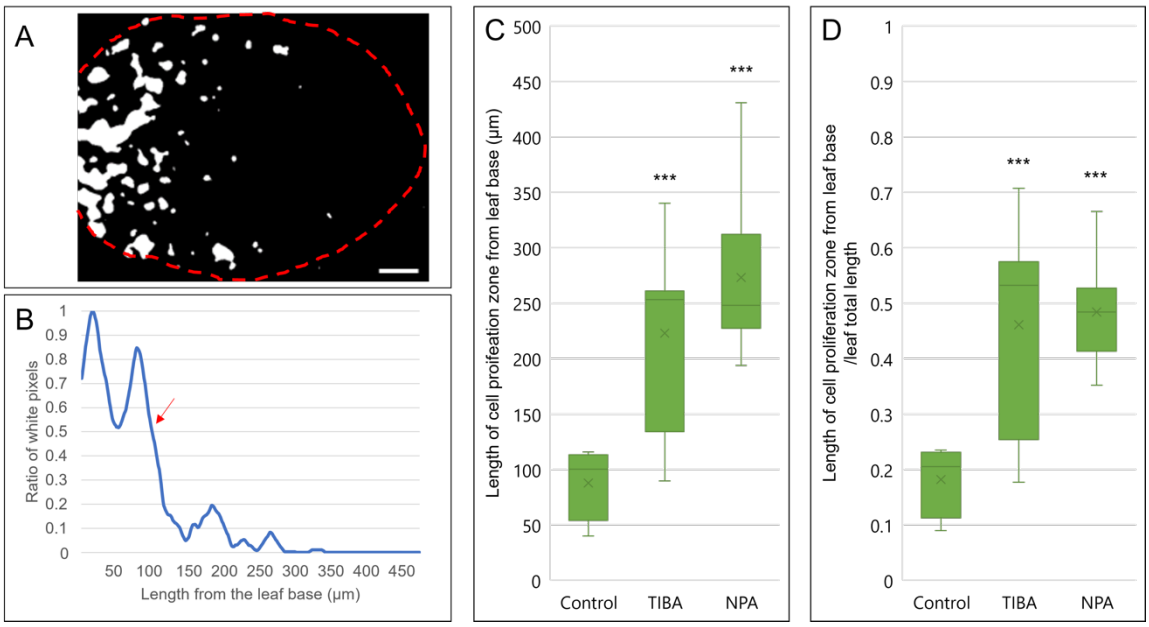

Fig. 3 Determination of cell proliferation zone and length and the ratio of cell proliferation occupying leaf primordia.

A: Binary images of GUS-stained leaf primordia. Scale bar: 50 μm.

B: The ratio of white pixels from a binary image was calculated, and the length of the cell proliferation zone (more than 50% of the white pixels) was determined. The red arrow indicates the end of the cell proliferation zone.

C: Length of cell proliferation zone from the leaf base.

D: The ratio of cell proliferation zone to the total leaf length.

n = 8, Dunnett's test, ***: $p < 0.001$

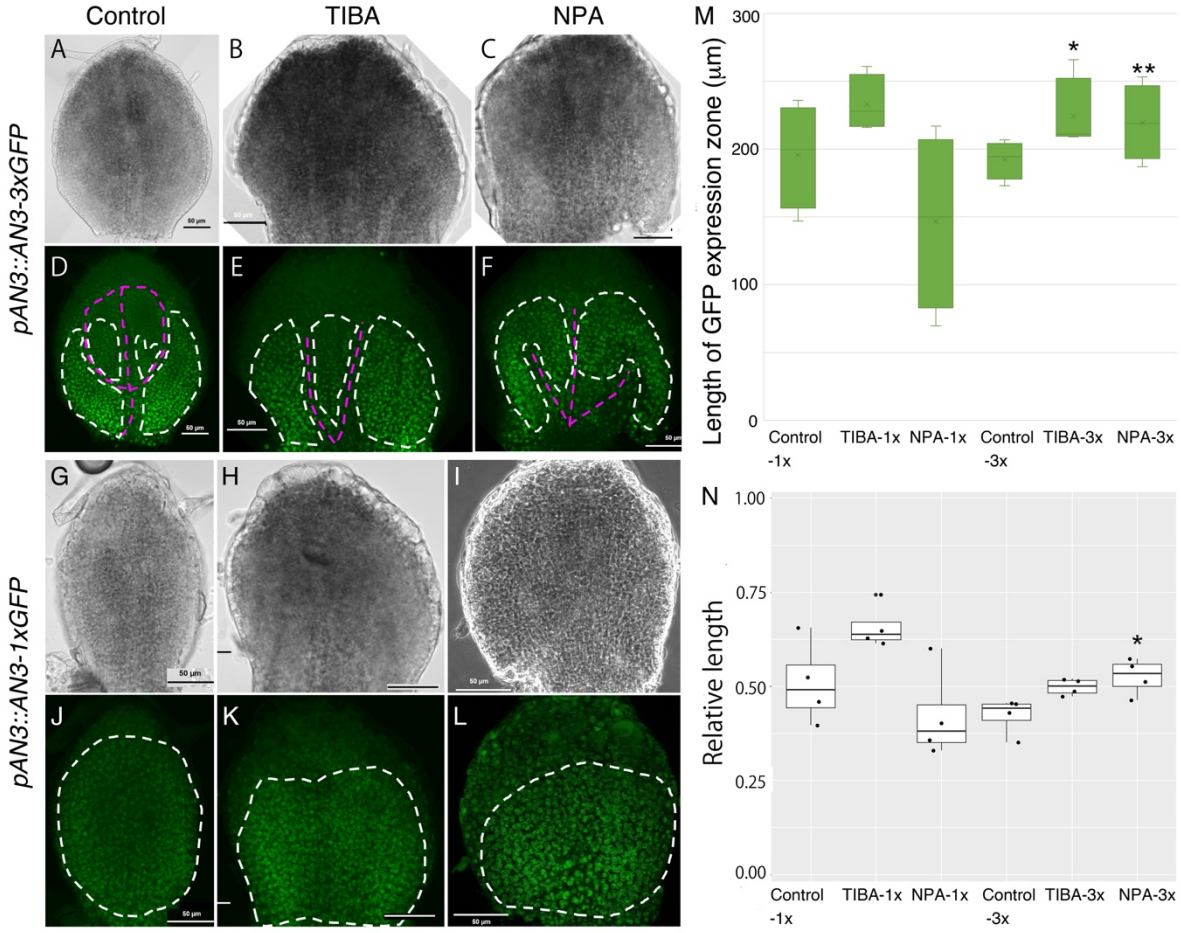

Fig. 4 GFP localization of *an3/pAtAN3::AN3-3xGFP* (A-F) and *an3/pAtAN3::AN3-GFP* (G-L), and their ratio of AN3-3xGFP and AN3-1xGFP localized area to the total length of leaf primordia.

Control (A, D, G, J), TIBA-treated (B, E, H, K), and NPA-treated (C, F, I, L) leaf primordia (5 DAS) are shown.

White dotted lines indicate GFP-localized area, and magenta lines indicate vasculature.

M indicates the actual length of GFP expression zone measured from leaf base. From left, *an3/pAtAN3::AN3-GFP* Control, TIBA and NPA; *an3/pAtAN3::AN3-3xGFP* Control, TIBA and NPA. n = 4, Dunnett's test, *: $p < 0.05$, **: $p < 0.001$

N indicates a ratio of AN3 mRNA and protein-localized area to the total length of leaf primordia. From left, *an3/pAtAN3::AN3-GFP* Control, TIBA and NPA; *an3/pAtAN3::AN3-3xGFP* Control, TIBA and NPA. n = 4, Dunnett's test, *: $p < 0.05$. No mark implies no statistically significant difference was observed.

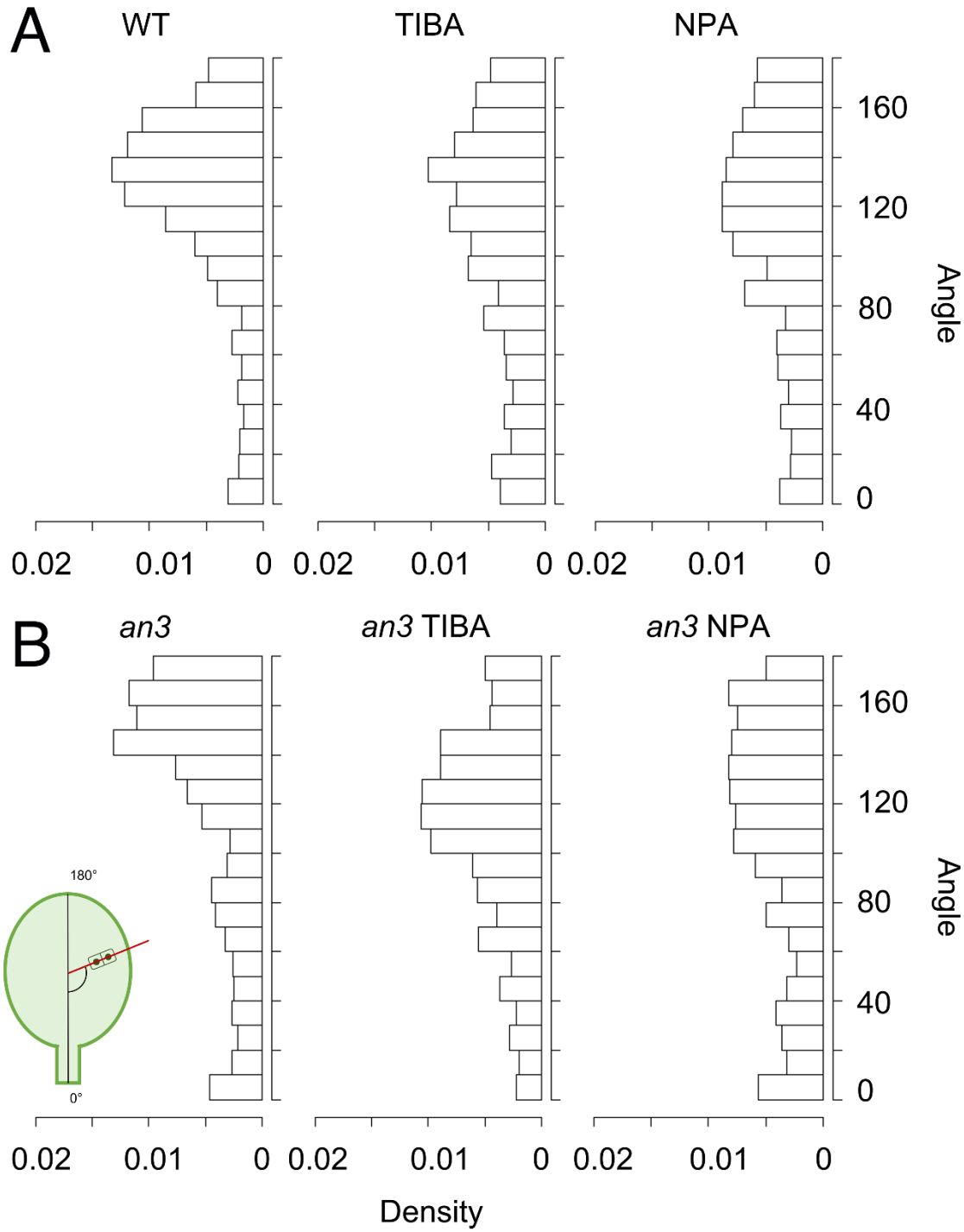

Fig. 5 Cell division angles in leaves. Four samples were investigated for each condition. A: From left, WT, TIBA, NPA; 1221, 1158, 1061 pairs of cells were analyzed, respectively. B: From left, *an3* mutant, TIBA (*an3* mutant), NPA (*an3* mutant); 971, 703 and 604 pairs of cells were analyzed, respectively. A schematic view of the angle measurements is inserted at the lower left.

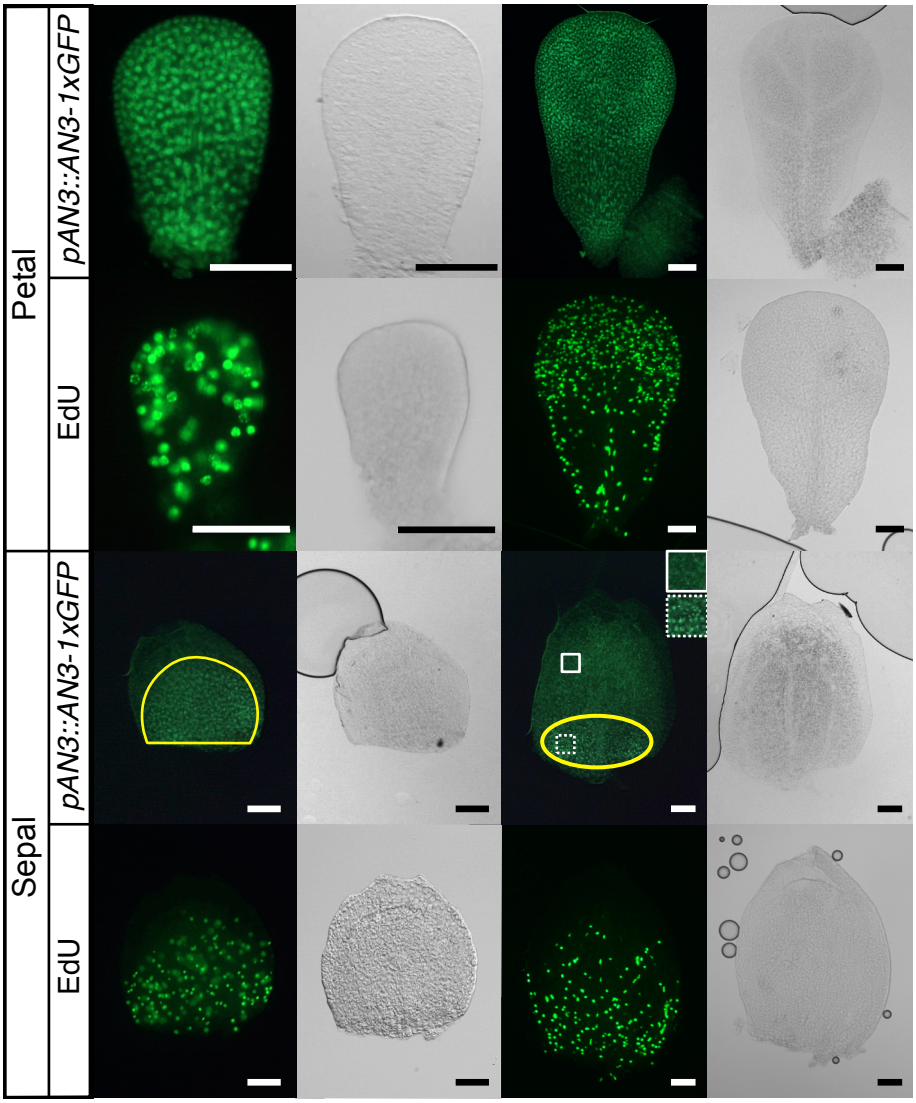

Fig. 6 AN3-1xGFP signals and EdU staining in sepal and petal primordia.
The primordia in the left two columns are younger than that in the right two columns. The stage of flower from which each primordium was collected is as follows: petal left, early stage 9; petal right, stage 1; sepal left, stage 7 (approx. 250 µm); sepal right stage 8 (approx. 450 µm). Normal transmitted light microscope images are shown on the right side of each fluorescent microscope image. Images of an AN3-GFP line are in the first row of each floral organ. The second row shows the floral primordia from the wild type treated with EdU. The yellow line shows areas with brighter AN3-1xGFP signals than the other part of the area in the primordia. Magnified views in each square of the sepal primordium are shown on the upper right.
Bar = 50 µm

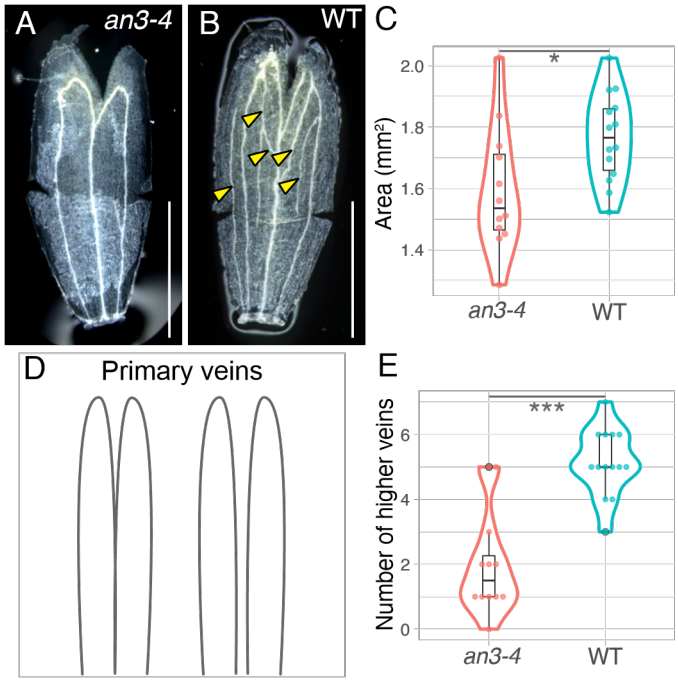

745

746 **Fig. 7** Phenotype of the sepal in the *an3-4* and the wild type. (A, B) Images of the sepal in
747 each genotype, *an3-4*, and the wild type. Some cuts were made to flatten the organs. The
748 yellow arrowheads point to the higher veins in the sepal. (C) The area of sepals in each
749 genotype. (D) Two patterns of primary veins are defined in this study. (E) The number of
750 higher veins of the sepals in each genotype. * $p < 0.05$, *** $p < 0.001$, Bar = 500 μm.

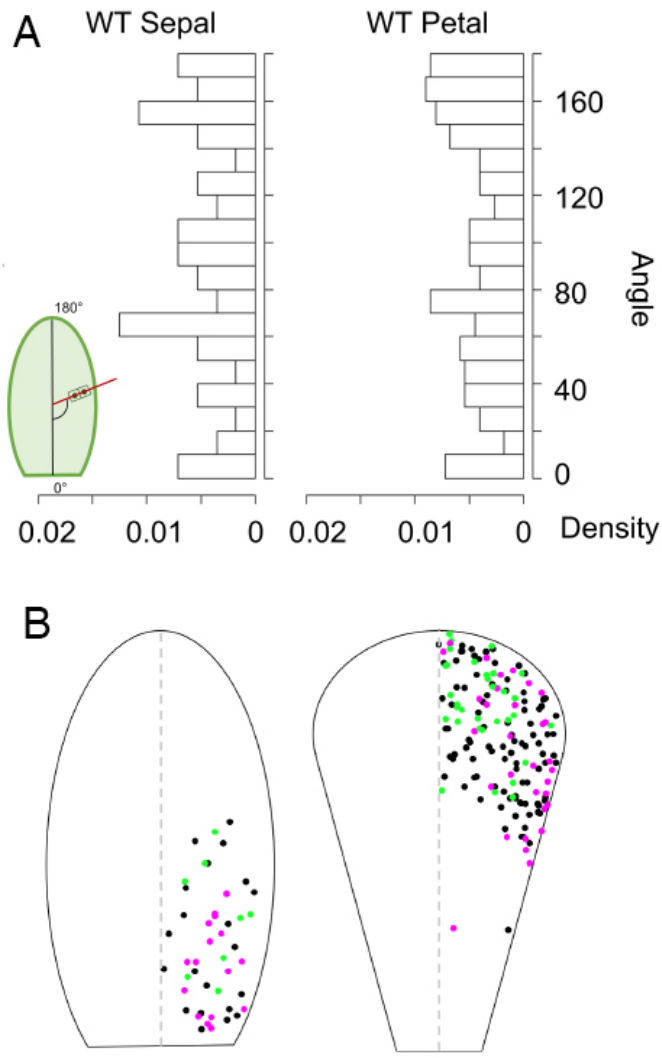

Fig. 8 Cell division angles in floral organs.

(A) From left, WT sepal, WT petal; 56 and 222 pairs of cells from four samples were analyzed, respectively. A schematic view of the angle measurements is inserted in the left corner. (B) Cell division angle distribution in floral organs. Left: sepal; 46 pairs of cells from three primordia were analyzed. Right: petal; 159 pairs of cells from three primordia were analyzed. The angles are mapped to the right half of the diagram, as the organs are symmetrical. The magenta dots indicate the cell division angle in 140°–180° (the upper peak in the panel A), the green dots indicate 60°-90° (the lower peak in the panel A), and the black dots indicate the angles that are in neither peak. n = 3